Superlattices and Microstructures 48 (2010) 31–40

Contents lists available at ScienceDirect

Superlattices and Microstructures

journal homepage: www.elsevier.com/locate/superlattices

Spin-flip effects in a parallel-coupled double quantum dot molecule

X.F. Yang [a,b], Y.S. Liu [a,b,*]

[a] Jiangsu Laboratory of Advanced Functional Materials, Changshu Institute of Technology, Changshu 215500, China
[b] College of Physics and Engineering, Changshu Institute of Technology, Changshu 215500, China

ARTICLE INFO

Article history:
Received 15 January 2010
Received in revised form
19 April 2010
Accepted 21 April 2010
Available online 21 May 2010

Keywords:
Spin-flip effects
Quantum dots
Fano effects

ABSTRACT

We investigate theoretically the electronic transport through a parallel-coupled double quantum dot (DQD) molecule attached to metallic electrodes, in which the spin-flip scattering on each quantum dot is considered. Special attention is paid to the effects of the intradot spin-flip processes on the linear conductance by using the equation of motion approach for Green's functions. When a weak spin-flip scattering on each quantum dot is present, the single Fano peak splits into two Fano peaks, and the Breit–Wigner resonance may be suppressed slightly. When the spin-flip scattering strength on each quantum dot becomes strong, the linear conductance spectrum consists of two Breit–Wigner peaks and two Fano peaks due to the quantum interference effects. The positions and shapes of these resonant peaks can be controlled by using the magnetic flux through the quantum device.

1. Introduction

Owing to the rapid development in the nanofabrication of quantum devices, electronic transport through mesoscopic quantum dots has been an interesting subject of experimental and theoretical works in the past decades [1–4]. In particular, two coupled quantum dots often form an artificial molecular system, which can be connected to the source and drain electrodes in either series or parallel configurations for studying the transport properties. Holleitner et al. [5] presented a quantum device with two coupled quantum dots embedded in an Aharonov–Bohm ring, and a flux-periodic current was detected in the case of the weakly coupled quantum dots. More recently,

* Corresponding author. Tel.: +86 0512 52251558.
E-mail address: ysliu2007@yahoo.com.cn (Y.S. Liu).

0749-6036/$ – see front matter © 2010 Elsevier Ltd. All rights reserved.
doi:10.1016/j.spmi.2010.04.010

extensive theoretical works on electronic transport through a DQD molecule connected in a parallel configuration to the metallic electrodes have been reported [6–11]. As a consequence of the quantum interference effects, a Breit–Wigner peak and a Fano peak appear in the linear conductance spectrum. The positions and widths of the two resonant peaks can be controlled by tuning the magnetic flux through the quantum device.

When the spin–orbit interaction on the quantum dot is taken into account, the spin rotation of an electron may happen. Some interesting quantum phenomena in the transport properties of quantum dot systems may be observed; for example, the single Kondo resonant peak splits into a two-peak or three-peak structure when the spin-flip scattering strength on the quantum dot is comparable with the Kondo temperature for a single quantum dot [12]. Cao et al. [13] studied the spin-dependent transport through a single quantum dot connected to a ferromagnet and a superconductor, where the spin-flip scattering on the quantum dot was included. The results showed that a single Andreev reflection (AR) conductance peak was developed when a weak spin-flip scattering was present. With the spin-flip scattering strength increasing, the single AR conductance peak developed into a double-peak structure in the conductance spectrum. Li et al. [14] studied the spin-dependent AR conductance tunneling through a T-shaped quantum dot sandwiched between a ferromagnet and a superconductor within the nonequilibrium Green's function, and the same intradot spin-flip scattering strength on each quantum dot was considered. The results of the study showed that the number of resonance peaks of the AR conductance increased, and the height of the AR conductance peaks was suppressed with the spin-flip scattering strength increasing.

In recent years, many theoretical suggestions have been proposed for the implementation of quantum dot systems in quantum computation and quantum information domains [15,16]. In particular, a quantum controlled-NOT (CNOT) gate was proposed by using the electron orbital states in a double coupled quantum dot system [17–19]. The reason is that the double coupled quantum dots often produce bonding and antibonding molecular states due to the interdot tunneling coupling like a molecule with two atoms. In this paper, we investigate theoretically the linear conductance of a parallel-coupled DQD molecule attached to metallic electrodes by using the equation of motion approach for Green's functions, where the same intradot spin-flip scattering strength is present. We mainly focus on the effect of spin-flip scattering in the DQD on the linear conductance at zero temperature. When a weak spin-flip scattering on each quantum dot is present, the single Fano peak splits into two Fano peaks, and the Breit–Wigner peak is suppressed slightly. Once the spin-flip scattering on each quantum dot becomes strong, the linear conductance spectrum consists of two Breit–Wigner peaks and two Fano peaks due to the quantum interference effects.

2. Model and method

The quantum device under consideration is shown in Fig. 1, in which only one electron energy level inside each quantum dot is considered due to the small size of the quantum dots. The spin-flip scattering on each quantum dot is included in the quantum model. We neglect the interdot and intradot electron–electron interactions in the quantum dot system, and the assumption is reasonable because the Coulomb energies are one order of the magnitude bigger than the coupling between the quantum dots and the metallic electrodes [20]. The magnetic flux Φ is applied perpendicular to the quantum device, which induces the phase-shift between the electron waves propagating in the clockwise and anticlockwise directions. The total Hamiltonian of the parallel-coupled DQD interferometer can be written as

$$H = H_{leads} + H_{center} + H_T. \tag{1}$$

The first term (H_{leads}) in Eq. (1), describing the left and right metallic electrodes in the noninteracting electron approximation, has the following expression:

$$H_{leads} = \sum_{\alpha=L,R;\ k\sigma} \epsilon_{\alpha k\sigma} a^{\dagger}_{\alpha k\sigma} a_{\alpha k\sigma}, \tag{2}$$

where $a^{\dagger}_{\alpha k\sigma}$ ($a_{\alpha k\sigma}$) denotes the creation (annihilation) operator for an electron with energy $\epsilon_{\alpha k\sigma}$ and spin index σ in the electrode α. The second term in Eq. (1) describes the dynamics of the double

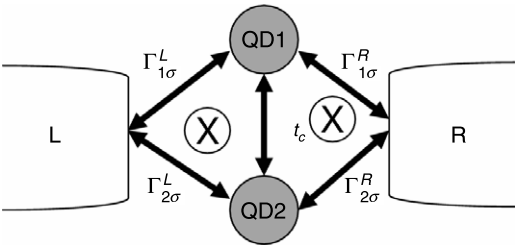

Fig. 1. Schematic plot of a parallel-coupled double quantum dot system with interdot tunneling t_c attached to the metallic electrodes. $\Gamma^{\alpha}_{j\sigma}$ ($j = 1, 2; \alpha = L, R; \sigma = \uparrow, \downarrow$) is the tunneling coupling between the jth quantum dot and the metallic electrode α.

coupled quantum dots in the center region, which can be modeled by a noninteracting two-site Anderson Hamiltonian,

$$H_{center} = \sum_{j\sigma} \epsilon_j d^{\dagger}_{j\sigma} d_{j\sigma} - \sum_{\sigma} t_c (d^{\dagger}_{1\sigma} d_{2\sigma} + h.c.) - R \sum_{j=1}^{2} (d^{\dagger}_{j\uparrow} d_{j\downarrow} + h.c.), \tag{3}$$

where R denotes the spin-flip scattering strength on each quantum dot, and $d^{\dagger}_{j\sigma}$ ($d_{j\sigma}$) creates (destroys) an electron with the energy ϵ_j and spin index σ in the jth quantum dot. t_c is the interdot coupling strength between two quantum dots. The third term in Eq. (1) represents the tunneling coupling between two quantum dots and the metallic electrodes, which is divided into two parts,

$$H_T = H^L_T + H^R_T. \tag{4}$$

H^{α}_T, describing the tunneling coupling between the center region and the electrode α, is written as

$$H^{\alpha}_T = \sum_{k,\sigma,\alpha} [(V_{\alpha 1\sigma} d^{\dagger}_{1\sigma} + V_{\alpha 2\sigma} d^{\dagger}_{2\sigma}) a_{\alpha k\sigma} + h.c], \tag{5}$$

where the tunneling matrix element $V_{\alpha j\sigma}$ ($j = 1, 2$) is assumed to be independent of k, and it can be written as $V_{L1\sigma} = |V_{L1\sigma}|e^{i\phi/4}$, $V_{L2\sigma} = |V_{L2\sigma}|e^{-i\phi/4}$, $V_{R1\sigma} = |V_{R1\sigma}|e^{-i\phi/4}$, $V_{R2\sigma} = |V_{R2\sigma}|e^{i\phi/4}$, with the AB phase $\phi = 2\pi\Phi/\Phi_0$ and the flux quantum $\Phi_0 = h/e$. Φ can be calculated by the formula $\Phi = B \cdot S$, where B is the magnetic field and S is the corresponding area of the quantum ring consisting of the double quantum dots and metallic electrodes. The value S may be obtained in the previous well-known experimental work, and it is 2.52×10^{-13} m^2 [5]. So the magnitude of the magnetic field B is 16.4 mT for $\phi = 2\pi$. The linewidth matrices $\mathbf{\Gamma}^L$ and $\mathbf{\Gamma}^R$ are given by

$$\mathbf{\Gamma}^L = \begin{pmatrix} \Gamma^L_{1\uparrow} & 0 & \sqrt{\Gamma^L_{1\uparrow}\Gamma^L_{2\uparrow}}e^{i\phi/2} & 0 \\ 0 & \Gamma^L_{1\downarrow} & 0 & \sqrt{\Gamma^L_{1\downarrow}\Gamma^L_{2\downarrow}}e^{i\phi/2} \\ \sqrt{\Gamma^L_{1\uparrow}\Gamma^L_{2\uparrow}}e^{-i\phi/2} & 0 & \Gamma^L_{2\uparrow} & 0 \\ 0 & \sqrt{\Gamma^L_{1\downarrow}\Gamma^L_{2\downarrow}}e^{-i\phi/2} & 0 & \Gamma^L_{2\downarrow} \end{pmatrix}, \tag{6}$$

and

$$\mathbf{\Gamma}^R = \begin{pmatrix} \Gamma^R_{1\uparrow} & 0 & \sqrt{\Gamma^R_{1\uparrow}\Gamma^R_{2\uparrow}}e^{-i\phi/2} & 0 \\ 0 & \Gamma^R_{1\downarrow} & 0 & \sqrt{\Gamma^R_{1\downarrow}\Gamma^R_{2\downarrow}}e^{-i\phi/2} \\ \sqrt{\Gamma^R_{1\uparrow}\Gamma^R_{2\uparrow}}e^{i\phi/2} & 0 & \Gamma^R_{2\uparrow} & 0 \\ 0 & \sqrt{\Gamma^R_{1\downarrow}\Gamma^R_{2\downarrow}}e^{i\phi/2} & 0 & \Gamma^R_{2\downarrow} \end{pmatrix}, \tag{7}$$

with the linewidth matrix $\Gamma^{\alpha}_{j\sigma} = \sum_k |V_{\alpha j\sigma}|^2 2\pi\delta(\epsilon - \epsilon_{\alpha k\sigma})$ ($\alpha = L, R; j = 1, 2; \sigma = \uparrow, \downarrow$).

The linear conductance σ is related to the total transmission $\tau(\epsilon)$ by the following formula at zero temperature [21]:

$$\sigma = \frac{e^2}{h}\tau(\epsilon) = \frac{e^2}{h}Tr[\mathbf{\Gamma}^L\mathbf{G}^r\mathbf{\Gamma}^R\mathbf{G}^a]. \tag{8}$$

In order to obtain the linear conductance σ, we need use the equation of motion approach for the retarded Green's function $\mathbf{G}^r(\epsilon)$, which is the Fourier transform of the retarded Green's function $\mathbf{G}^r(t-t')$,

$$\mathbf{G}^r(t-t') = -\mathrm{i}\theta(t-t')\langle\{\Psi(t), \Psi^\dagger(t')\}\rangle, \tag{9}$$

where the quantum operator $\Psi^\dagger = (d_{1\uparrow}, d_{1\downarrow}, d_{2\uparrow}, d_{2\downarrow})^\dagger$. g^r is defined as the Fourier-transformed retarded Green's function of the center region without the coupling to two metallic electrodes, which is written as

$$[g^r(\epsilon)]^{-1} = \begin{pmatrix} \epsilon-\epsilon_1+\mathrm{i}0^+ & R & t_c & 0 \\ R & \epsilon-\epsilon_1+\mathrm{i}0^+ & 0 & t_c \\ t_c & 0 & \epsilon-\epsilon_2+\mathrm{i}0^+ & R \\ 0 & t_c & R & \epsilon-\epsilon_2+\mathrm{i}0^+ \end{pmatrix}. \tag{10}$$

By employing the matrix Dyson's equation, the retarded Green's function $\mathbf{G}^r(\epsilon)$ can be written as

$$\mathbf{G}^r(\epsilon) = \{[g^r(\epsilon)]^{-1} - \mathbf{\Sigma}^r(\epsilon)\}^{-1}, \tag{11}$$

where $\mathbf{\Sigma}^r(\epsilon)$ is the retarded self-energy matrix from the tunneling coupling between the DQD molecule and two metallic electrodes. Under the wide-bandwidth approximation, one can obtain the relation $\mathbf{\Sigma}^r = -\frac{i}{2}(\mathbf{\Gamma}^L + \mathbf{\Gamma}^R)$.

Once the retarded Green's function is obtained, the advanced Green's function can be obtained by the relation $\mathbf{G}^a(\epsilon) = [\mathbf{G}^r(\epsilon)]^+$. The total local density of states (LDOS) is calculated by using the diagonal matrix elements of the retarded Green's function $\rho = -\frac{1}{\pi}\sum_{j=1}^{4}\mathrm{Im}\,\mathbf{G}^r_{jj}(\epsilon)$.

3. Results and discussions

The results and discussions of the present studies will be presented in this section. For simplicity, a perfectly symmetrical system with parameters $\Gamma^\alpha_{j\sigma} = \Gamma_0(\alpha = L, R; j = 1, 2; \sigma = \uparrow, \downarrow)$ is chosen in this paper. For many practical systems, Γ_0 is the order of meV [22,23], while in this work we concentrate on the spin-flip scattering in the DQD at zero temperature so that Γ_0 is set to be the reference unit of energy. When the spin-flip scattering on each quantum dot is ignored, such a quantum model has been studied extensively in numerous previous literatures [6–11]. In the case of no magnetic flux through the quantum device, the width of the Fano resonance becomes zero. The reason is that the antibonding state is decoupled from the two metallic electrodes due to the destructive quantum interference [8,9]. Once the magnetic field is switched on, the Fano peak will come back. In this paper, we will focus on the effects of the spin-flip on the linear conductance in a parallel-coupled double quantum dot Aharonov–Bohm interferometer at zero temperature.

We first study the transport properties of a parallel-coupled double quantum dot Aharonov–Bohm interferometer under weak spin-flip scattering strengths ($R \ll \Gamma_0$); the linear conductance can be obtained by the Landauer formula (Eq. (8)). In the upper plane in Fig. 2, we plot the linear conductance σ as a function of the Fermi energy E_F under several different values of the weaker spin-flip scattering. For simplification, the system parameters for the numerical calculations are assumed as $\epsilon_1 = \epsilon_2 = \epsilon_0 = \Gamma_0$, $t_c = \Gamma_0$ and $\phi = 0.3\pi$, respectively. Due to the interdot tunneling coupling t_c and spin-flip scattering R, four coherent molecular states are developed at energies $\epsilon_0 - t_c - R$, $\epsilon_0 - t_c + R$, $\epsilon_0 + t_c - R$, and $\epsilon_0 + t_c + R$, respectively. In particular, when $R = 0$, the linear conductance spectrum is composed of one Breit–Wigner peak located around $\epsilon_0 - t_c$ and one Fano peak located around $\epsilon_0 + t_c$, as shown in the upper plane of Fig. 2 (see the solid line) [9]. In this case, the linear conductance σ in

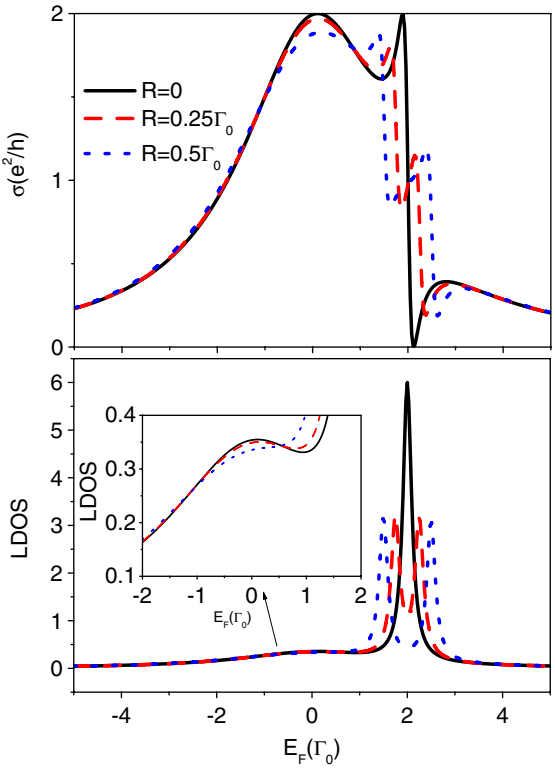

Fig. 2. (Color online) Linear conductance σ and LDOS ρ as functions of the Fermi energy E_F for different values of the weak spin-flip scattering R. The system parameters are chosen as $\epsilon_1 = \epsilon_2 = \epsilon_0 = \Gamma_0$, $\phi = 0.3\pi$ and $t_c = \Gamma_0$, respectively.

the Breit–Wigner region can be approximated as

$$\sigma \simeq \frac{2e^2}{h}\frac{1}{e_+^2+1}, \tag{12}$$

and the linear conductance σ in the Fano-like region has the following approximate expression:

$$\sigma \simeq \frac{2e^2}{h}T_b\frac{(q+e_-)^2}{e_-^2+1}, \tag{13}$$

where $e_\pm = (E_F - \epsilon_0 \pm t_c)/\Gamma_\pm$ with $\Gamma_\pm = \Gamma_0[1 \pm \cos(\phi/2)]$, $T_b = 1/(1+q^2)$, and $q = -2t_c/\Gamma_+$. In this paper, we are mainly interested in the dependence of the linear conductance on the spin-flip scattering strengths on each quantum dot. When the weaker spin-flip scattering is present, the single Fano peak develops into a double-peak structure, and the positions of the two Fano peaks are located around $\epsilon_0 + t_c \pm R$ (see the upper plane of Fig. 2). The reason for this is that the quantum state giving rise to the Fano peak is a weakly coupled electronic state, and it is more sensitive to the spin-flip scattering strength. With the spin-flip scattering increasing, the two small Fano peaks move in the opposite directions, and the height of the Breit–Wigner peak is suppressed slightly. There is no double-peak structure appearing around $\epsilon_0 - t_c$ in the linear conductance spectrum due to the strongly coupled electronic state corresponding to the Breit–Wigner resonance. In order to interpret the numerical results, the corresponding LDOS as a function of the Fermi energy is plotted in the bottom plane of Fig. 2. We find that the total LDOS peak around $\epsilon_0 + t_c$ splits into two LDOS peaks, while the LDOS peak around $\epsilon_0 - t_c$ is suppressed slightly. As a result, the single Fano-like peak splits into two Fano-like

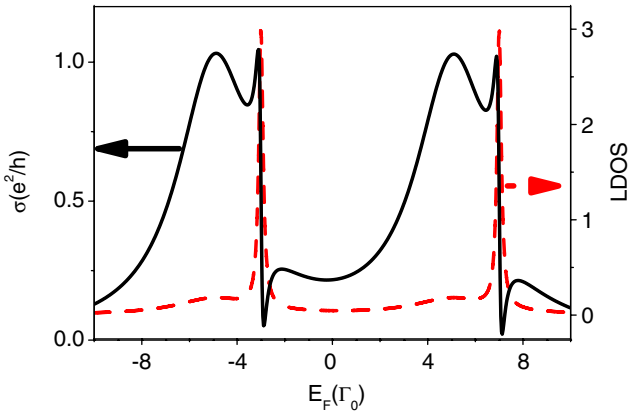

Fig. 3. (Color online) Linear conductance σ (black solid line) and LDOS ρ (red dashed line) as functions of the Fermi energy E_F for strong spin-flip scattering $R = 5\Gamma_0$. The other system parameters are chosen as those in Fig. 2.

peaks in the presence of weak spin-flip scattering, while the Breit–Wigner resonance is suppressed slightly.

Now we begin with the study of the effects of strong spin-flip scattering on the transport properties of a double quantum dot Aharonov–Bohm interferometer. The linear conductance σ (the left axis) and the total LDOS ρ (the right axis) as functions of the Fermi energy with the strong spin-flip scattering on each quantum dot are illustrated in Fig. 3. The spin-flip scattering is taken as $R = 5\Gamma_0$, and the other system parameters are chosen as those in Fig. 2. The results show that two wider LDOS peaks appear around $\epsilon_0 - t_c \pm R$, which give rise to two Breit–Wigner peaks in the conductance spectrum. Two narrow LDOS peaks are located in the vicinity of the energies $\epsilon_0 + t_c \pm R$, which induce two Fano peaks in the conductance spectrum. The reason is that quantum interference effects happen when electron transport takes place through weakly coupled electronic states at energies $\epsilon_0 + t_c \pm R$ and strongly coupled electronic states at energies $\epsilon_0 - t_c \pm R$.

The periodic oscillation of the linear conductance as a function of the magnetic flux is an important phenomenon when the phase coherence of electrons in a parallel-coupled double quantum dot Aharonov–Bohm interferometer is preserved. In Fig. 4, we plot the dependence of the linear conductance σ on the magnetic flux ϕ. The upper plane shows σ versus the Fermi energy E_F and the magnetic flux ϕ. The spin-flip scattering R is chosen as $7\Gamma_0$, and other system parameters are taken as those in Fig. 2. We note that the linear conductance is a periodic function of ϕ with a period of 4π, which is readily explained by the different electron-transmission pathways [6]. It is interesting to note that the two Breit–Wigner peaks and two Fano peaks can be interchanged by tuning the magnetic flux ϕ. In particular, we plot the linear conductance σ as a function of E_F for the magnetic flux $\phi = 0.3\pi$ and 1.7π in the bottom plane of Fig. 4. The two Breit–Wigner peaks evolve into two Fano peaks, while the two Fano peaks develop into two Breit–Wigner peaks when the magnetic flux varies from 0.3π to 1.7π. Such a swap effect among four molecular states in a parallel-coupled double quantum dot Aharonov–Bohm interferometer with strong spin-flip scattering may be applied to future quantum computation.

The dependence of the linear conductance σ on the Fermi energy E_F in the absence of the interdot tunneling coupling $t_c = 0$ is shown in Fig. 5, and other system parameters are chosen as in Fig. 2. The linear conductance σ as a function of the Fermi energy E_F is plotted in the upper plane for several different values of the spin-flip scattering R. When $R = 0$, the linear conductance has the following expression:

$$\sigma(E_F, \phi) = \frac{2e^2}{h} \frac{4\Gamma_0^2 (E_F - \epsilon_0)^2 \cos^2(\frac{\phi}{2})}{[(E_F - \epsilon_0)^2 - \Gamma_0^2 \sin^2(\phi/2)]^2 + 4\Gamma_0^2 (E_F - \epsilon_0)^2}. \tag{14}$$

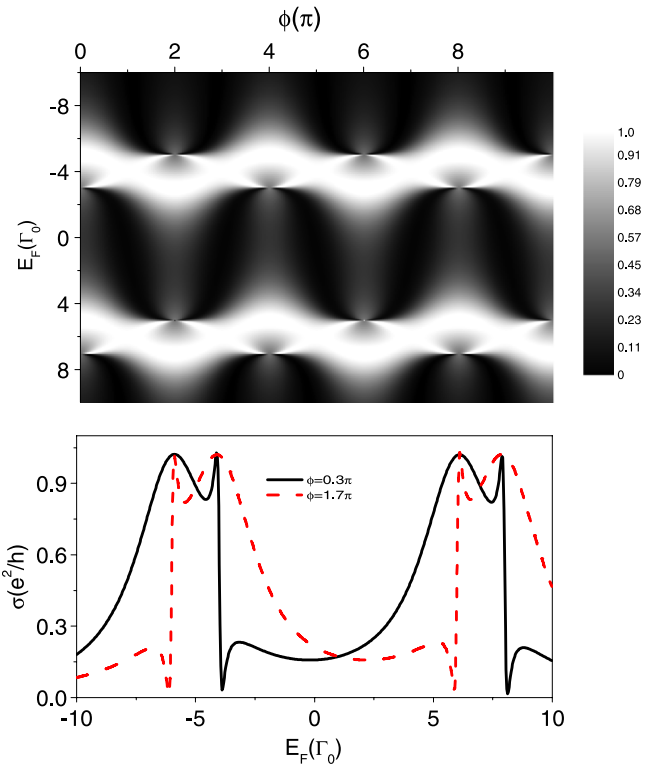

Fig. 4. (Color online) Upper plane: linear conductance σ as a function of the Fermi energy E_F and magnetic flux ϕ. Lower plane: linear conductance σ as a function of the Fermi energy E_F for different magnetic fluxes ϕ. The other system parameters are chosen as those in Fig. 2.

From the above equation, we can see clearly that the zero conductance point appears at the energy ϵ_0 due to the destructive quantum interference effect, and there are two resonant peaks located at $\epsilon_0 \pm \Gamma_0 \sin(\phi/2)$ (see the solid line in the upper plane of Fig. 5). When the spin-flip scattering is present, the zero conductance point at the energy ϵ_0 disappears, and two new conductance dips appear at energies $\epsilon_0 - R$ and $\epsilon_0 + R$ in the linear conductance spectrum due to spin-flip scattering strength on each quantum dot, and four resonant peaks appear at around $\epsilon_0 \pm R \pm \Gamma_0 \sin(\phi/2)$. We also plot the linear conductance σ as a function of the Fermi energy E_F in the lower plane for different values of the magnetic flux. The height of the linear conductance σ is suppressed with the increasing of the magnetic flux due to $\sigma \propto \cos^2(\frac{\phi}{2})$ even in the presence of spin-flip scattering on each quantum dot, and the linear conductance disappears when $\phi = \pi$.

Finally, we plot the linear conductance σ and LDOS ρ as functions of the quantum dot energy levels ϵ_1 and ϵ_2 with the fixed spin-flip scattering $R = 5\Gamma_0$ in Fig. 6. Here the interdot tunneling is absent, and the quantum dot level can be tuned experimentally by using the voltage applied on the quantum dot. The magnetic flux through the quantum device is chosen to be $\phi = 0$. When $R = 0$, the quantum dot system is the same as the system proposed in the previous work [6]. In the following calculation, the Fermi energy is fixed at the zero of energy. The results show that quantum dot levels and spin-flip scattering can significantly influence the transport properties of a double quantum dot Aharonov–Bohm interferometer. The linear conductance is symmetrical on the line $\epsilon_1 = \epsilon_2$, and two perfect tunneling channels with linear conductance approaching $2e^2/h$ are opened in the points $(5\Gamma_0, -5\Gamma_0)$ and $(-5\Gamma_0, 5\Gamma_0)$, as shown in the upper plane of Fig. 6. The numerical results can be explained by the following analytical expressions. When $\epsilon_1 = R$, the linear conductance σ can be

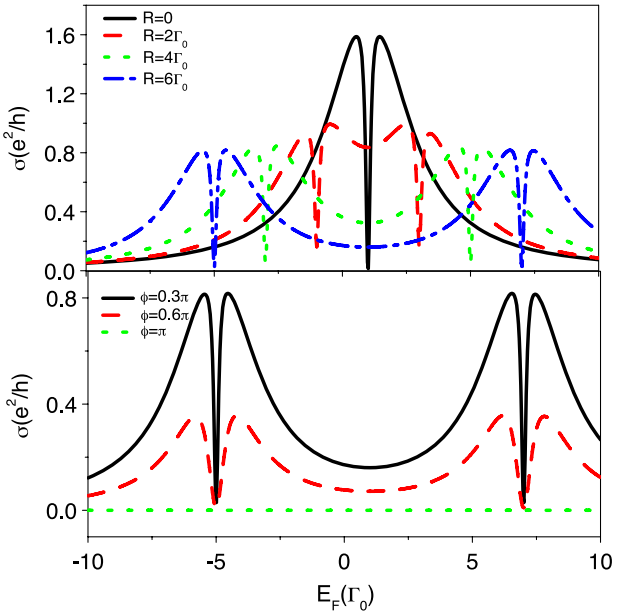

Fig. 5. (Color online) Linear conductance σ as a function of the Fermi energy E_F in the absence of the interdot tunneling coupling $t_c = 0$. The upper plane corresponds to several different values of spin-flip scattering R, and the lower plane represents the case with several different magnetic fluxes ϕ.

written as

$$\sigma(\epsilon_2) = \frac{2e^2}{h}\frac{2R^2(\epsilon_2+R)^2 + (\epsilon_2+3R)^2\Gamma_0^2}{4R^2(\epsilon_2+R)^2 + (\epsilon_2+3R)^2\Gamma_0^2}. \tag{15}$$

The above equation shows clearly that the linear conductance has a resonance peak with $\sigma = 2e^2/h$ at $\epsilon_2 = -R$ such that a perfect tunneling channel is opened at the point $(R, -R)$, and the other perfect tunneling channel can be found at the point $(-R, R)$. We also find that Fano-line-shape resonances appear in the vicinity of points $(-R, -R)$ and (R, R) due to quantum interference effects (see the upper plane of Fig. 6), and the physical reason for this is that the corresponding high-LDOS peaks appear in the vicinity of points $(-R, -R)$ and (R, R) as shown in the lower plane of Fig. 6.

4. Summary

In summary, we have investigated theoretically the linear conductance properties of a parallel-coupled DQD molecule sandwiched between two metallic electrodes at zero temperature based on the equation of motion approach for Green's functions, in which the intradot spin-flip scattering on each quantum dot has been taken into account. We focus on the effects of the intradot spin-flip processes on the transport properties. When a weak spin-flip scattering on each quantum dot is present, the single Fano peak splits into two peaks, and the Breit–Wigner peak is suppressed slightly. When strong spin-flip scattering on each dot is present, the linear conductance spectrum may be decomposed into two Breit–Wigner peaks and two Fano peaks due to quantum interference effects. A swap effect among the four molecular states is also found by controlling the magnetic flux threading through the quantum device.

Acknowledgements

The authors are grateful for support from the National Natural Science Foundation of China (NSFC) under Grant No. 10947130 and the Science Foundation of the Education Committee of Jiangsu Province

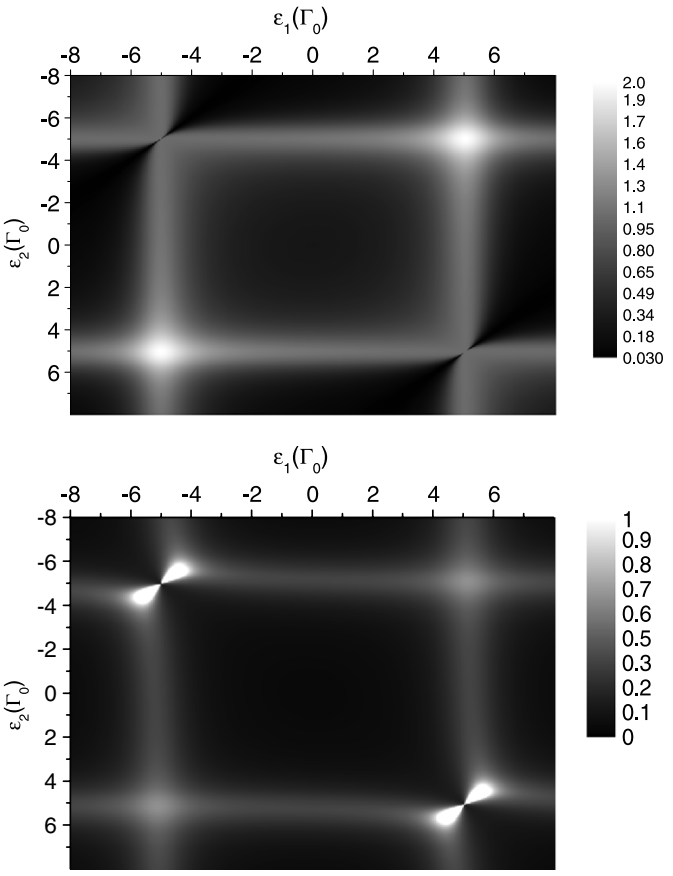

Fig. 6. Linear conductance σ (the upper plane) and the total LDOS ρ (the lower plane) as functions of the energy levels of two quantum dots ϵ_1 and ϵ_2.

under Grant No. 09KJB140001. The authors are also grateful for the support of the Foundations of Changshu Institute of Technology.

References

[1] W. Liang, M. Bockrath, H. Park, Phys. Rev. Lett. 88 (2002) 126801.
[2] For a review see for example W.G. van der Wiel, S. De Franceschi, J.M. Elzerman, S. Tarucha, T. Fujisawa, L.P. Kouwenhoven, Rev. Mod. Phys. 75 (1) (2003).
[3] Y.S. Liu, H. Chen, X.H. Fan, X.F. Yang, Phys. Rev. B 73 (2006) 115310.
[4] Y.S. Liu, H. Chen, X.F. Yang, J. Phys.: Condens. Matter 19 (2007) 246201.
[5] A.W. Holleitner, C.R. Decker, H. Qin, K. Eberl, R.H. Blick, Phys. Rev. Lett. 87 (2001) 256802.
[6] B. Kubala, J. Könjg, Phys. Rev. B 65 (2002) 245301.
[7] Z.M. Bai, M.F. Yang, Y.C. Chen, J. Phys.: Condens. Matter 16 (2004) 2053.
[8] M.L. Ladrón de Guevara, F. Claro, P.A. Orellana, Phys. Rev. B 67 (2003) 195335.
[9] P.A. Orellana, M.L. Ladrón de Guevara, F. Claro, Phys. Rev. B 70 (2005) 233315.
[10] H.Z. Lu, R. Lü, B.F. Zhu, Phys. Rev. B 71 (2005) 235320.
[11] F. Chi, S.S. Li, J. Appl. Phys. 97 (2005) 123704.
[12] P. Zhang, Q.K. Xue, Y.P. Wang, X.C. Xie, Phys. Rev. Lett. 89 (2002) 286803.
[13] X.F. Cao, Y.M. Shi, X.L. Song, S.P. Zhou, H. Chen, Phys. Rev. B 70 (2004) 235341.
[14] Y.X. Li, H.Y. Choi, H.W. Lee, J.J. liu, J. Appl. Phys. 101 (2007) 103918.
[15] F. Troiani, U. Hohenester, E. Molinari, Phys. Rev. B 62 (2000) R2263.
[16] J.H. Oh, D. Ahn, S.W. Hwang, Phys. Rev. A 62 (2000) 052306.
[17] A. Barenco, D. Deutsch, A. Ekert, R. Jozsa, Phys. Rev. B 74 (1995) 4083.
[18] S. Moskal, S. Bednarek, J. Adamowski, Phys. Rev. A 71 (2005) 062327.

[19] S. Moskal, S. Bednarek, J. Adamowski, Phys. Rev. A 76 (2007) 032302.
[20] W.G. van der Wiel, S. De Franceschi, J.M. Elzerman, T. Fujisawa, S. Tarucha, L.P. Kouwenhoven, Rev. Mod. Phys. 75 (1) (2002).
[21] S. Datta, Electronic Transport in Mesoscopic System, Cambridge University Press, Cambridge, England, 1997.
[22] A. Matulis, F.M. Peeters, P. Vasilopoulos, Phys. Rev. Lett. 72 (1994) 1518.
[23] Y. Mu, Y. Fu, M. Willander, Superlattices Microstruct. 22 (1997) 135.